0888-8809/04/$15.00/0
Printed in U.S.A.

Molecular Endocrinology 18(11):2777–2789

doi: 10.1210/me.2004-0124

Key Amino Acids Located within the Transmembrane Domains 5 and 7 Account for the Pharmacological Specificity of the Human V1b Vasopressin Receptor

S. DERICK, A. PENA, T. DURROUX, J. WAGNON, C. SERRADEIL-LE GAL, M. HIBERT, D. ROGNAN, AND G. GUILLON

Institut National de la Santé et de la Recherche Médicale (INSERM) Unité 469 (S.D., A.P., T.D., G.G.), 34094 Montpellier, Cedex 05 France; Unité Mixte de Recherche (UMR), Centre National de la Recherche Scientifique (CNRS) 7081 (M.H., D.R.), F-67401 Illkirch, France; Sanofi-Synthélabo Recherche (J.W.), 31100 Toulouse, France; and Sanofi-Synthélabo Recherche (C.S.-L.G.), 34000 Montpellier, France

In mammals, the vasopressin V_{1b} receptor (V_{1b}-R) is known to regulate ACTH secretion and, more recently, stress and anxiety. The characterization of the molecular determinant responsible for its pharmacological selectivity was made possible by the recent discovery of the first V_{1b} antagonist, SSR149415. Based upon the structure of the crystallized bovine rhodopsin, we established a three-dimensional molecular model of interaction between the human V_{1b}-R (hV_{1b}-R) and SSR149415. Four amino acids located in distinct transmembrane helices (fourth, fifth, and seventh) were found potentially responsible for the hV_{1b}-R selectivity. To validate these assumptions, we selectively replaced the leucine 181, methionine 220, alanine 334, and serine 338 residues of hV_{1a}-R by their corresponding amino acids present in the hV_{1b}-R (phenylalanine 164, threonine 203, methionine 324, and asparagine 328, respectively). Four mutants, which all exhibited nanomolar affinities for vasopressin and good coupling to phospholipase C pathway, were generated. hV_{1a} receptors mutated at position 220 and 334 exhibited striking increase in affinity for SSR149415 both in binding and phospholipase C assays at variance with the hV_{1a}-R modified at position 181 or 338. In conclusion, this study provides the first structural features concerning the hV_{1b}-R and highlights the role of few specific residues in its pharmacological selectivity. (*Molecular Endocrinology* 18: 2777–2789, 2004)

VASOPRESSIN (AVP) IS A neurohypophysial hormone involved in a wide range of physiological actions including vasoconstriction, antidiuresis, and stimulation of ACTH (1), catecholamine (2), insulin, glucagon (3), and heart atrial natriuretic factor secretion (4). AVP is also supposed to regulate numerous central functions such as synaptic transmission, central control of body temperature, memory, and, more recently, anxiety and depression behaviors in the rat (5, 6).

This functional diversity is explained by interaction of AVP with three different specific receptor isoforms called V_{1a}, V_{1b}, and V_2, on the basis of their pharmacological and G protein-coupling properties (for review see Refs. 1 and 7). The V_{1a} and V_{1b} subtypes are positively coupled to phospholipase Cβ and involved mainly in blood pressure control and regulation of ACTH secretion, respectively. The V_2 AVP receptor is coupled to adenylyl cyclase and is responsible for the antidiuretic effect of AVP. All these three receptor isoforms have been cloned and sequenced (for review see Ref. 8). Whatever the species considered, they all share the structural characteristics of G protein-coupled receptors (GPCRs) including the seven α-helical transmembrane (TM) domains, which exhibit strong sequence similarities.

Over the past few years, many selective peptide and nonpeptide agonists or antagonists of AVP receptors exhibiting a good affinity have been characterized (9, 10). For example, SR49059 and d[$(CH_2)_5$Tyr(Me^2)]AVP are both potent and selective V_{1a} antagonists with nanomolar affinities in various species (9). Similarly, SR121463A is the best selective V_2 antagonist described (9). Very recently d[Cha^4]AVP and SSR149415 were characterized as the first specific agonist and antagonist of the V_{1b} isoform, respectively (6, 11).

Due to this wide range of physiological effects, high amino acid sequence homology, and complex phar-

Abbreviations: AVP, [8-Arginine]vasopressin; CHO, Chinese hamster ovary; 3D, three-dimensional; d[Cha^4]AVP, [1-deamino, 4-cyclohexylalanine]AVP; E2 loop, second extracellular loop; GA, genetic algorithm; GPCR, G protein-coupled receptor; HBS, Hanks' buffered saline; IP, inositol phosphate; rms, root mean square; TM, transmembrane; V_{1b}-R, vasopressin V_{1b} receptor.

***Molecular Endocrinology* is published monthly by The Endocrine Society (http://www.endo-society.org), the foremost professional society serving the endocrine community.**

macological properties, the AVP receptor family represents an interesting system to investigate the functional molecular determinants of G protein-coupled receptor isoforms. Previous studies performed on AVP V_{1a} and V_2 receptor subtypes (V_{1a}-R and V_2-R) have led to valuable information concerning the structure of the binding sites of many ligands. Thus, by mutational analysis and three-dimensional (3D) modeling, Mouillac and co-workers (12) have characterized the binding site of AVP in the human (h)V_{1a}-R. The hormone-binding site is located in a 15–20Å deep cleft surrounded by the top of the TM domains. Additional studies have further demonstrated that residues located in the first extracellular loop and in the N-terminal tail of the receptor also play a role in the binding of AVP (13, 14). Because of the high conservation of the residues involved in the interaction with the hormone, this binding site has been proposed to be common to the three AVP receptor subtypes (12). By using photoaffinity labeling, mutational analysis, and 3D molecular modeling approaches, structural information concerning the pharmacological specificity of the V_{1a} and V_2 receptor subtypes was also provided. These studies allowed the characterization of the binding sites of some V_{1a} and V_2 peptide or nonpeptide antagonists (15–18). They are located mainly in the top of the seventh TM domain (16), in the first (17) and second extracellular (E2) loops (15). Further studies performed on the V_{1a} and the V_2 receptors also led to the identification of residues that differentiate agonist *vs.* antagonist binding (14, 15, 19).

At variance with the V_{1a} and V_2 receptor isoforms, no structural information about the V_{1b} subtype is available. This lack of structural data is due mainly to the absence of V_{1b}-specific pharmacological tools. Very recently, we synthesized [1-deamino, 4-cyclohexylalanine]AVP (d[Cha^4]AVP), the first specific peptidic agonist of nanomolar affinity for the hV_{1b}-R (11). At the same time Serradeil-Le Gal *et al.* designed SSR149415, the first nonpeptide antagonist exhibiting an excellent affinity for this AVP receptor isoform (6). These selective pharmacological tools have allowed the discovery of new V_{1b}-R functions. This AVP receptor isoform was thus shown to control some emotional behaviors. On various tests performed in the rat, SSR149415 exhibits potent anxiolytic and antidepressive effects similar to those induced by classical benzodiazepines or antidepressant drugs (20). Such discovery was recently confirmed by the invalidation of this AVP receptor in mice (21). These animals devoid of V_{1b}-Rs displayed a less aggressive behavior as compared with control (21). At the peripheral level, the V_{1b}-Rs are also thought to be potent regulators of pancreas and adrenal functions by their ability to control insulin and catecholamine release respectively (22, 23). The V_{1b}-R may thus represent a new target for drugs of therapeutic interest especially for the treatment of affective disorders. A better understanding of its molecular structure and of the binding mode of its ligands may then represent an important challenge to design new selective and potent drugs.

The purpose of this work is to propose and validate a 3D molecular model of the interactions between the antagonist SSR149415 and the hV_{1b}-R and to characterize the molecular determinants responsible for its ligand selectivity.

RESULTS

Alignment of Amino Acid Sequences and 3D Molecular Modeling

Aligning the amino acid sequences of both hV_{1a} and hV_{1b} AVP receptor subtypes with that of bovine rhodopsin is rather straightforward as rhodopsin-like fingerprints (*e.g.* NPxxY at TM7; see Ref. 24) are common to the three receptors. Of the 32 TM residues (Fig. 1) supposed to map the TM binding cavity for receptor antagonists (25), only nine differ between V_{1a} and V_{1b} AVP receptor subtypes. Interestingly, four of these residues are clustered in TM7.

The current hV_{1b}-R model was derived directly from a previously reported V_{1a} model that proved useful to discriminate known V_{1a}-R antagonists from randomly chosen drug-like molecules by high-throughput virtual screening (25) and to unambiguously determine the binding mode of the selective V_{1a} antagonist SR49059 by covalent labeling (26). Automated docking of the selective V_{1b} antagonist SSR149415 suggests a binding mode between TMs 3, 5, 6, and 7 (Fig. 2, A and B). The three aromatic moieties of SSR149415 are embedded in three hydrophobic subsites (Fig. 2B). The hydroxyl group of SSR149415 H-bonds to Gln301 side chain, which is conserved for V_{1a} and V_{1b} receptor subtypes, and its amide oxygen atom H bonds to Thr203 side chain at TM5. Of the nine above-mentioned residues varying between hV_{1a} and hV_{1b} receptors, four amino acids (Phe164 on TM4, Thr203 on TM5, Met324 and Asn328 on TM7) are in close contact with SSR149415 in the proposed 3D model. Phe164 is unlikely to explain the V_{1b} selectivity of SSR149415 as it is mutated to a residue (Leu) in the V_{1a}-R that could interact similarly with the latter antagonist. The model suggests Thr203 and Met324 to be much more relevant. Hence, Thr203 and Met324 develop molecular interactions (H bond and hydrophobic contacts, respectively) with the V_{1b}-R, that are not possible with the V_{1a} subtype due to the observed amino acid mutations (Thr203 to Met, Met324 to Ala). Last, Asn328, which is part of the subsite predicted to interact with the dimethoxyphenyl moiety of SSR149415, and mutated to Ser in the V_{1a}-R, could also be a molecular determinant of the observed V_{1b} selectivity of the investigated antagonist. To validate these predictions, four residues (Phe164, Thr203, Met324, and Asn328) were thus selected for site-directed mutagenesis.

Fig. 1. Alignment of AVP V_{1a} and V_{1b} Receptor Sequences to that of Bovine Rhodopsin

The amino acid sequence of the human AVP receptor subtypes, V_{1a} (hV_{1a}-R) and V_{1b} (hV_{1b}-R), are compared with that of the bovine rhodopsin (OPSD BOVIN). TM helices (TM1–TM7) delimited by *dark bars* have been assigned as in the x-ray crystal structure of bovine rhodopsin (29). E1–E3 and I1–I3 indicate the position of extracellular and intracellular loops, respectively. Thirty-two residues the side chains of which are directed toward the TM binding cavity are displayed in *boldface*. Among these 32 positions, nine residues enclosed by a *box* differ between the V_{1a} and V_{1b} receptor subtypes.

Role of Specific Amino Acid Residues in hV_{1b}-R Selectivity: a Site-Directed Mutagenesis Approach

We selectively replaced the Leu181, Met220, Ala334, and Ser338 residues of hV_{1a}-R by their corresponding amino acids present in the hV_{1b}-R (Phe164,Thr203, Met324, and Asn328, respectively; Fig. 3). These mutants of the hV_{1a}-R were termed L181F, M220T, A334M, and S338N, respectively. As compared with the wild-type V_{1a}-R, they all bound [^{3}H]AVP with nanomolar affinities [dissociation constant (K_d)] and were expressed to similar levels (Table 1).

To validate the 3D model of interaction proposed above, we first determined the affinities of the mutated receptors generated for the specific V_{1b} nonpeptide antagonist SSR149415. As shown in Fig. 4 and Table 2, replacement in the hV_{1a}-R sequence of methionine 220 by a threonine residue increased the affinity of the mutant M220T for SSR149415 by 26-fold as compared with the wild-type hV_{1a}-R. Similarly, the A334M mutant also displayed a significant but more reduced shift of its affinity for the SSR149415 (8.9-fold gain in affinity as compared with the wild-type V_{1a}-R) (Fig. 4 and Table 2). The effects of these two single mutations were not additive because the double mutant M220T/A334M displayed an affinity for SSR149415 similar to that determined for the A334M mutant (Table 2). By contrast, the L181F mutant did not exhibit any significant gain in affinity for the specific V_{1b} antagonist (Fig. 4 and Table 2). For the S338N mutant, we even observed a small (3.2-fold) decrease of affinity for the SSR149415 molecule. This decreased affinity could be explained by the probable loss of one hydrogen bond between the *p*-methoxy oxygen atom of the antagonist and the serine side chain, which is no longer possible with an asparagine (see Fig. 2).

We also decided to extend this pharmacological study to other specific AVP receptor-selective ligands. For the M220T mutant, the affinities of SR49059 and SR121463, two specific V_{1a} and V_2 nonpeptide antagonists, respectively (27, 28), were significantly decreased as compared with the wild-type hV_{1a}-R (Fig. 4 and Table 2). This was also the case for [^{125}I]-HO-LVA, a specific peptide V_{1a} antagonist and d[Cha^4]AVP, a specific peptide V_{1b} agonist. Conversely, the affinity of F-180, a specific V_{1a} peptide agonist, was not significantly modified (Fig. 4 and Table 2). The A334M mutant did not display such modifications. Its affinity for SR49049 was not strongly decreased. By contrast, that of SR121463 was significantly enhanced (6.2-fold gain in its affinity as compared with the wild-type hV_{1a}-R) (Table 2). This mutant also exhibited a weak, but significant, increase of its affinity for the selective V_{1b} agonist d[Cha^4]AVP (4.2-fold increase as compared with the wild-type hV_{1a}-R) (Fig. 4 and Table 2), and no modification for F-180. For the L181F and S338N mutants, no significant pharmacological differences concerning their affinities for the SR49059, SR121463, F-180, and d[Cha^4]AVP analogs were observed.

The ability of the M220T and A334M mutants to stimulate phospholipase C activity was further evaluated on Chinese hamster ovary (CHO)-transfected cells. Whatever the mutant considered (M220T or A334M), AVP was shown to stimulate accumulation of inositol phosphates (IPs) in a dose-dependent manner with the same activity constants (K_{act}) as compared with wild-type AVP receptors (Fig. 5A and Table 3). The ability of SSR149415 to antagonize the AVP-

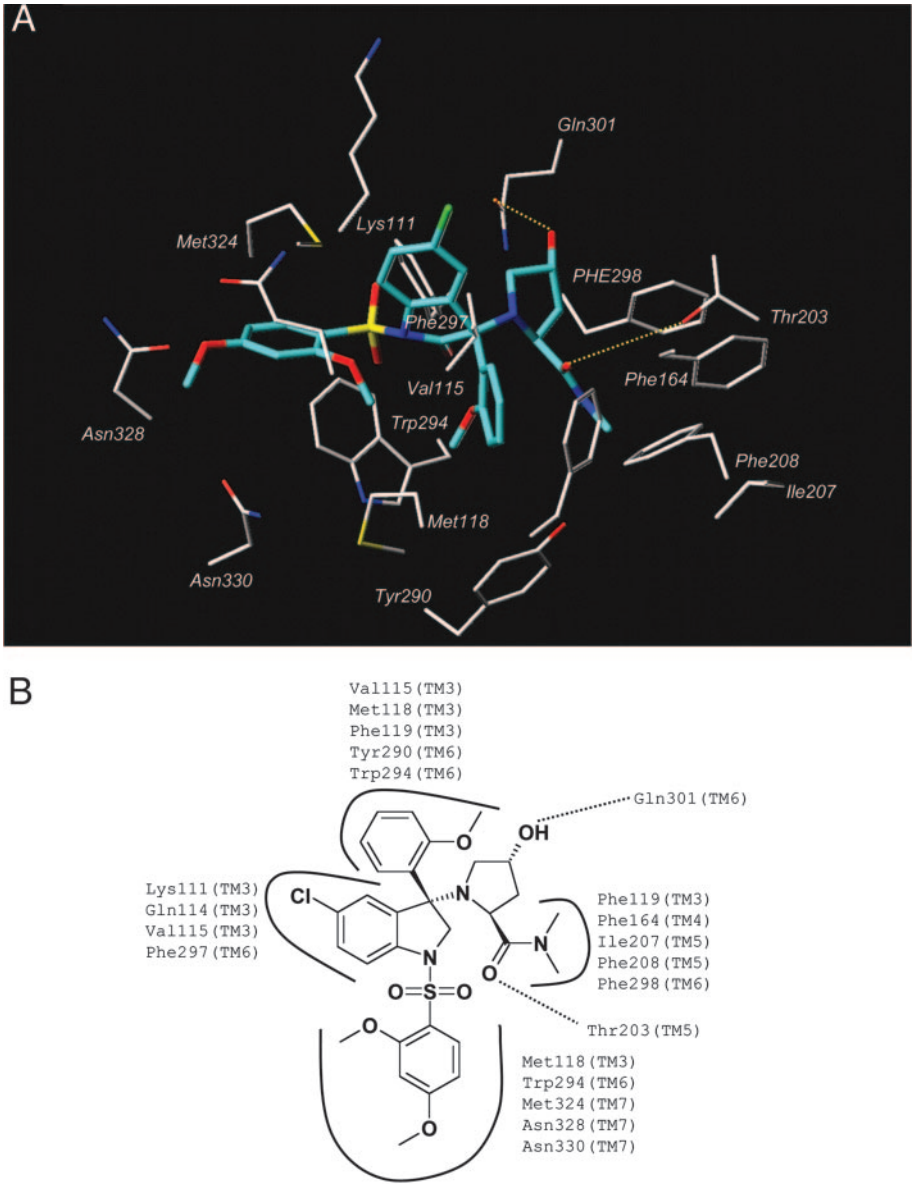

Fig. 2. SSR149415 Docked into the Binding Cavity of hV_{1b}-R

A, As described in *Materials and Methods*, the Gold 1.2 docking program (41) was used to automatically dock the selective V_{1b} antagonist SR149415. The best solution proposed by the Gold program is illustrated (fitness score of 41.16). Residues are numbered according to their position in the primary sequence of the hV_{1b}-R. *Cyan and white sticks* display carbon atoms of the SSR149415 compound and of the V_{1b}-R, respectively. B, Schematic view of the interaction model. Putative intermolecular H-bonds are displayed by *dotted lines*. All residues potentially interacting with the different parts of the nonpeptide SSR149415 are shown. Numbering of the residues and of the TM helices is identical to the one used in panel A. Intermolecular H-bonds are displayed by *dotted lines*. *Numbers in parentheses* indicate the TM helix to which the current residue belongs.

induced IP response was further investigated. As expected and illustrated on Fig. 5B, the potency of SSR149415 to inhibit AVP-stimulated IP accumulation was strongly affected as compared with CHO cells expressing wild-type AVP receptors. The inhibition constants (K_{inact}) of SSR149415 for M220T and A334M mutants were 36.5- and 4.6-fold reduced, respectively, as compared with wild-type hV_{1a}-R (Table 3).

Potential Role of the E2 Loop in hV_{1b}-R Selectivity: a Chimeric Approach

The roles of some extracellular loops of the V_{1a} and V_2 receptors in ligand binding has been previously demonstrated (13, 15). We thus hypothesized that the E2 loop may also be involved in the hV_{1b}-R selectivity because its amino acid sequence varied from one AVP receptor isoform to another. To validate this hypothe-

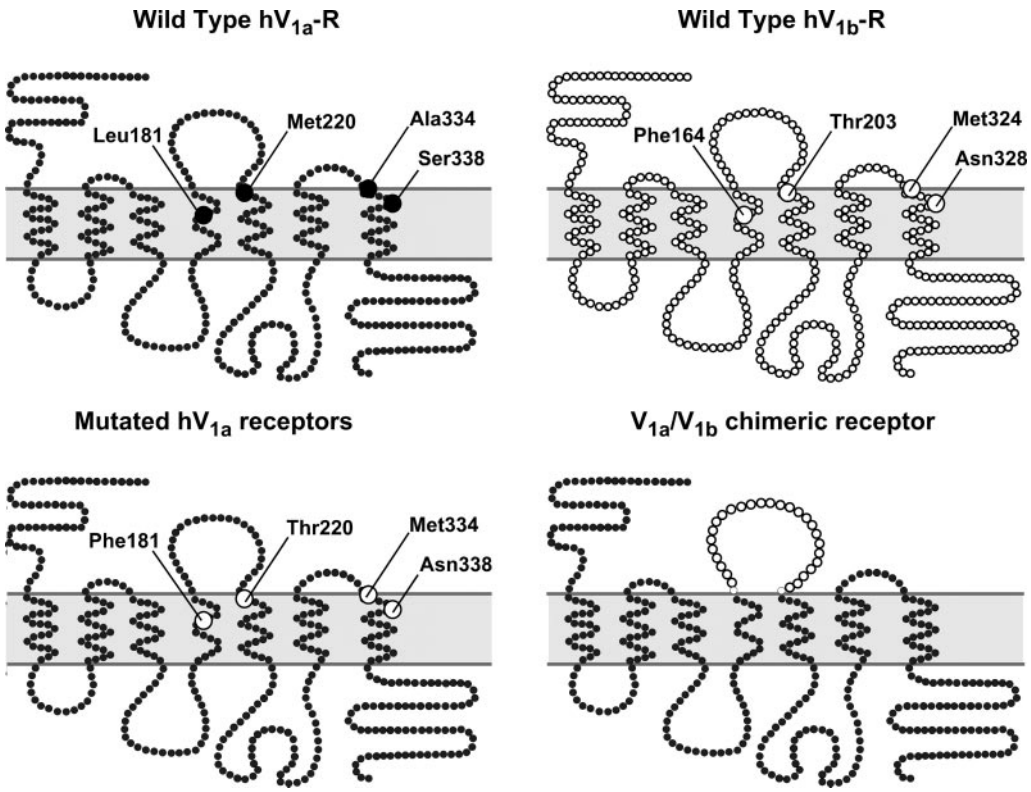

Fig. 3. Schematic Representation of Wild-Type, Mutant, and Chimeric AVP Receptors Used in This Study

Black and white circles represent amino acids from the wild-type hV_{1b} and the hV_{1a} receptors, respectively. *Lower left panel*, Single mutant of each amino acid modified and double mutant of the 220 and 334 residues generated. *Lower right panel*, $V_{1a}/E2V_{1b}$ chimeric receptor.

Table 1. Binding Properties of Wild-Type and Mutant AVP Receptors for [^{3}H]AVP

AVP Receptor	K_d (nM)	B_{max} (fmol/mg protein)
Wild-type receptors		
V_{1a}	0.44 ± 0.05	994 ± 77
V_{1b}	0.49 ± 0.06	2714 ± 559
Single- and double-mutant receptors		
L181F	0.70 ± 0.27	700 ± 280
M220T	0.68 ± 0.06	706 ± 168
A334M	0.96 ± 0.16	943 ± 127
S338N	0.57 ± 0.13	890 ± 193
M220T/A334M	0.60 ± 0.08	368 ± 66
Chimeric receptor		
$V_{1a}/E2V_{1b}$	0.66 ± 0.05	451 ± 94

Membranes from CHO cells expressing human wild-type V_{1a}, V_{1b} receptors and L181F, M220T, A334M, S338N, M220T/A334M, $V_{1a}/E2V_{1b}$ V_{1a} mutated receptors, were incubated with increasing amounts of [^{3}H]AVP in the presence (nonspecific binding) or absence (total binding) of 1 μM unlabeled AVP as described in *Materials and Methods.* Specific binding was calculated. The dissociation constant (K_d) and the maximal binding capacity (B_{max}) of each AVP receptor were determined from Scatchard representation as described in *Materials and Methods.* Data are the mean ± SEM of at least three separate experiments each performed in triplicate.

sis, we replaced the wild-type hV_{1a}-R E2 loop by the hV_{1b}-R counterpart (Fig. 3). Saturation binding experiments showed that the resulting chimeric receptor ($V_{1a}/E2V_{1b}$) bound [^{3}H]AVP with a nanomolar affinity (Table 1). Unfortunately, competition experiments did not reveal any significant modifications of its affinity whatever the selective VP analogs tested (Table 2).

DISCUSSION

This study describes, for the first time, some structural features concerning the hV_{1b}-R and provides information about its interaction with the selective nonpeptide antagonist SSR149415.

First we developed a 3D molecular model of the hV_{1b}-R. This model integrates 1) the structural data from Palczewski *et al.* (29) concerning the bovine rhodopsin, the first crystallized GPCR and 2) information from the 3D model of the hV_{1a}-R recently published and validated (26). The docking of SSR149415 into the hV_{1b}-R molecular model was performed as previously described for SR49059 into the hV_{1a}-R using the Gold program. From this interaction model, it was proposed that only four amino acid residues in close contact with SSR149415 and differing between the hV_{1b} and the

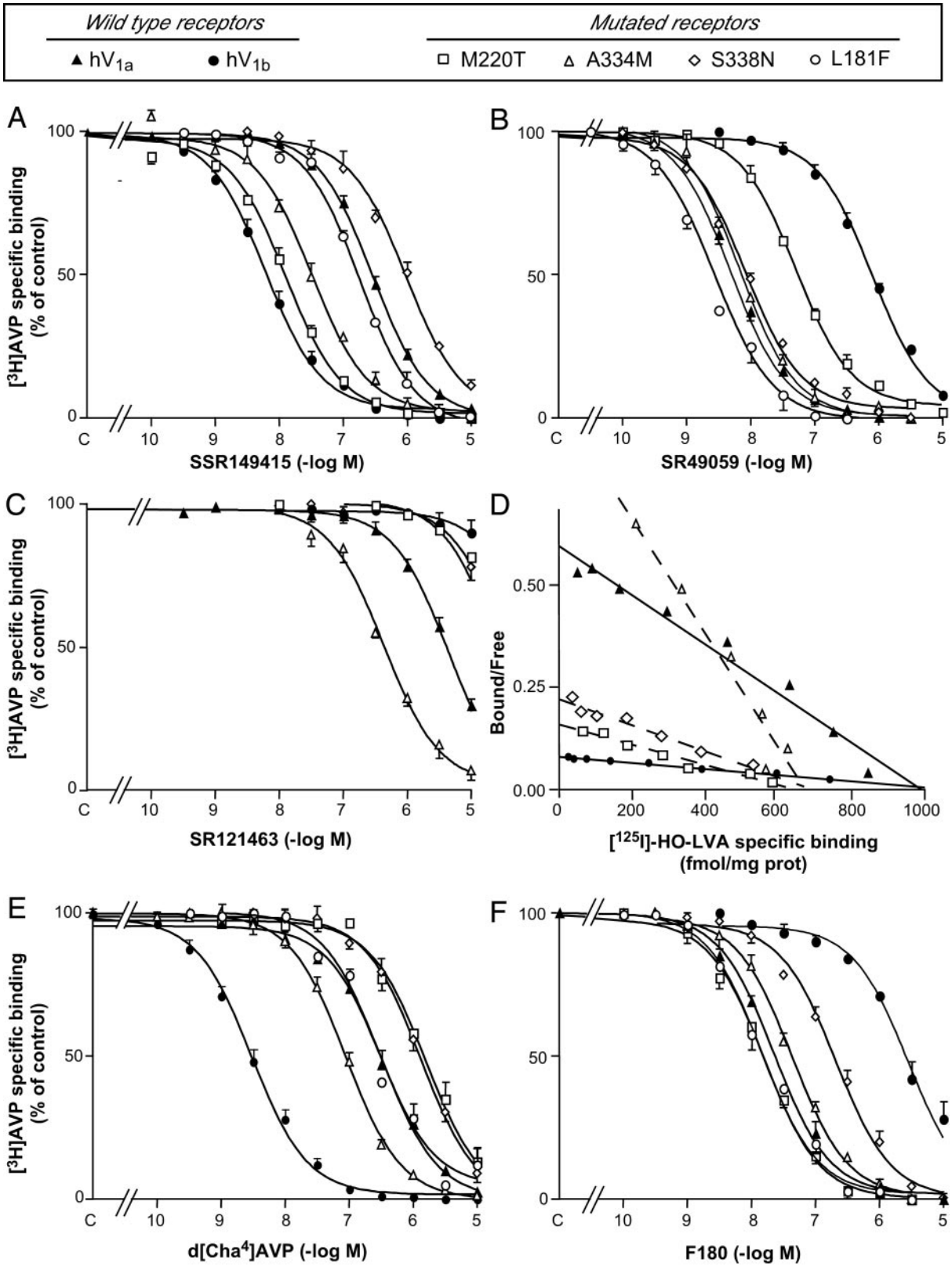

Fig. 4. Binding Properties of Wild-Type and Mutant AVP Receptors

A, B, C, E, and F, Membrane preparations of CHO cells expressing the human wild-type V_{1a} (▲), V_{1b} (●) receptor and the L181F (○)M220T (□), A334M (△), S338N (◇), M220T/A334M, and V_{1a}/E2V_{1b} mutated receptors were incubated as described in *Materials and Methods* with 0.5–1 nM [^{3}H]AVP in the absence (C, control) or in the presence of increasing amounts of unlabeled SSR149415, SR49059, SR121463, d[Cha^4]AVP, or F-180. Specific binding, measured in each condition, is expressed as percent of control

Table 2. Binding Properties of Wild-Type and Mutant AVP Receptors for Various Selective AVP Receptor Compounds

AVP Receptor	Affinity (nM)					
	Antagonists				Agonists	
	SSR149415[a]	SR49059[a]	SR121463[a]	[^{125}I]-OH-LVA[b]	d[Cha^4]AVP[a]	F-180[a]
Wild-type receptors						
V_{1a}	110 ± 11	1.82 ± 0.11	1131 ± 117	0.031 ± 0.005	151 ± 11[c]	11.7 ± 0.2[d]
V_{1b}	2.65 ± 0.35	262 ± 21	>5000	0.35 ± 0.02	1.2 ± 0.1[c]	2100 ± 800[d]
Single- and double-mutant receptors						
L181F	90.8 ± 3.4	1.0 ± 0.2	nd	nd	151 ± 18	7.5 ± 0.8
M220T	4.24 ± 0.29	17.5 ± 1.0	>5000	0.110 ± 0.004	534 ± 8	6.0 ± 0.7
A334M	12.4 ± 1.7	3.81 ± 0.51	183 ± 15	0.014 ± 0.002	35.9 ± 6.0	17.5 ± 1.9
S338N	348 ± 98	3.33 ± 0.45	>5000	0.076 ± 0.003	483 ± 94	51.1 ± 8.3
M220T/A334M	11.3 ± 1.8	nd	nd	0.066 ± 0.008	532 ± 72	nd
Chimeric receptor						
V_{1a}/E2V_{1b}	150 ± 70	1.1 ± 0.2	686 ± 67	0.017 ± 0.003	292 ± 60	11.7 ± 0.4

Binding assays were performed as described in *Materials and Methods.* K_i values ([a]) were calculated from dose-displacement curves illustrated in Fig. 4. K_d values of [^{125}I]-HO-LVA ([b]) were determined as previously described for [^{3}H]AVP, from saturation experiments not illustrated in this study. Data are the mean ± SEM of at least three separate experiments each performed in triplicate.

[c,d] Previous data reported in Refs. 11 and 42, respectively. nd, Not determined.

hV_{1a} receptors may be potentially involved in the V_{1b} selectivity of SSR149415: Phe164, Thr203, Met324, and Asn328. Site-directed mutagenesis and analysis of the binding and functional properties of the resulting mutants revealed that Phe164, the side chain of which points outward of the binding crevice in our current V_{1a} and V_{1b} models, is not involved in the V_{1b} selectivity as well as Asn328. By contrast, Thr203 and/or the Met324 residues represent the minimal structural motif responsible for the selectivity of hV_{1b}-R for SSR149415. This selectivity derives probably from the abilities of the Thr203 and Met324 amino acids to establish H bond and hydrophobic interactions, respectively, with the SSR149415 compound as suggested by the interaction model proposed (see Fig. 2). We also might expect to observe an increase of the affinity of the double mutant for SSR149415. Its seems difficult to explain this nonadditivity of effects at the molecular level. Yet, as the M220T mutation contributes to enlarge the cavity around the TM5, whereas the A334M mutation limits the size of a remote subsite at TM7, it is possible that the double mutant undergoes small conformational rearrangements to optimize the packing of the TM7 bundle that slightly decreases the affinity of the selective V_{1b} antagonist SSR149415 for the double mutant.

Interestingly, although the selective V_{1a} antagonist SR49059 and the selective V_{1b} antagonist SSR149415 share a common structure, they are proposed to bind to their cognate receptor in a very different manner (Fig. 6). The indoline ring of SSR149415 is embedded in a hydrophobic pocket located between TMs 3 and 6, whereas the corresponding scaffold in SR49059 interacts mainly with TM5. Likewise, the dimethoxyphenyl moiety of SSR149415 is essentially directed toward TM7, whereas that of SR49059 mainly interacts with TMs 5 and 6 (Fig. 6). Last, the prolinamide moieties of both antagonists are located in opposite directions in the TM cavity of both AVP receptors (Fig. 6). The main two positions demonstrated to control V_{1b} selectivity are located at opposite extremities of the antagonist binding cavity (Thr203 on TM5, Met324 on TM7) and are spatially distant from approximately 18 Å (measured from the Cα atoms). These two positions, 5.42 and 7.39 in the Ballesteros numbering (30), are key determinants of most GPCR antagonist-binding sites (31).

The current V_{1b}-SSR149415 3D model, as well as the recently described V_{1a}-SR49059 model (38), provides a good explanation for the herein reported mutation effects at the above cited two positions. Assuming a conserved binding mode of one individual antagonist to both receptors, the M220T mutation in the V_{1a}-R favors the binding of SSR149415 by creation of an additional H-bonding site for the prolinamide moiety, whereas the A334M mutation will reinforce the hydrophobic interactions to the dimethoxyphenyl group (Fig. 6). Conversely, the latter mutations will

specific binding, and fitted according to the Cheng and Prusoff equation (see *Materials and Methods*). Data are the mean ± SEM of three separated experiments each performed in triplicate. D, The same membrane preparations were incubated with increasing amounts of [^{125}I]-HO-LVA with (nonspecific binding) or without (total binding) 1 μM unlabeled AVP. Specific binding was calculated and Scatchard representation illustrated (see *Materials and Methods*). Experimental values are from one representative experiment performed in triplicate.

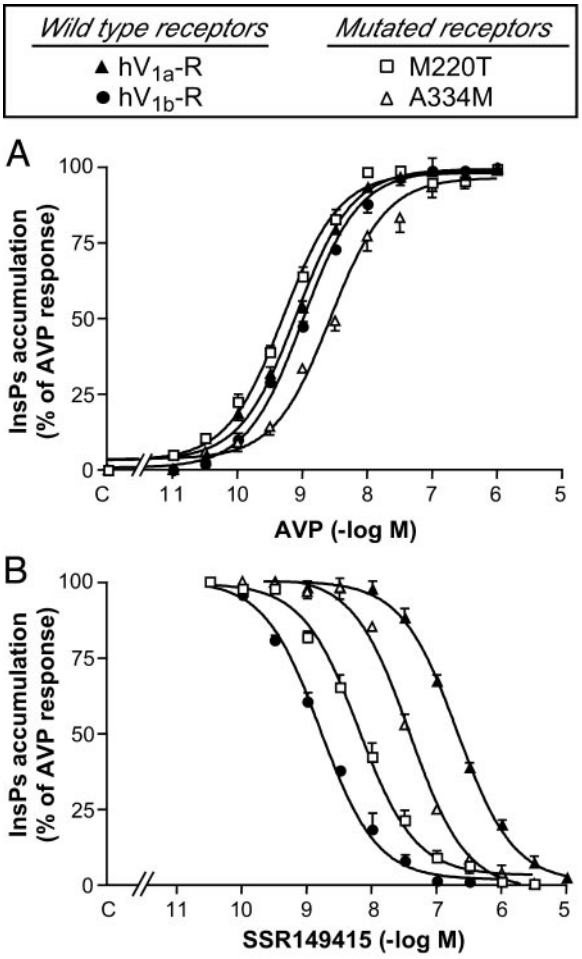

Fig. 5. Functional Properties of Wild-Type and Mutant AVP Receptors

CHO cells expressing the human wild-type V_{1a} (▲), V_{1b} (●) receptor, or the M220T (□), A334M (△) mutated receptors were labeled with 1 μCi myo-[2-^{3}H]inositol. Cells were incubated with either increasing amounts of AVP (*upper panel*) or preincubated with increasing amounts of SSR149415 and further stimulated with 1 nM AVP as described in *Materials and Methods* (*lower panel*). Total IPs accumulated were extracted, counted, and expressed as percent of the maximal response induced by 1 μM AVP (*upper panel*) or 1 nM AVP without antagonist (*lower panel*). Results are the mean ± SEM of at least three distinct experiments each performed in triplicate.

disfavor binding of the selective V_{1a} antagonist SR49059 by increasing the size and hydrophilicity of the lipohilic cavity around its indoline ring (M220T mutation in V_{1a} residue numbering), and creating steric clashes with the prolinamide moiety (A334M).

Yet, both the M220T and A334M mutants, the affinity of which for SSR149415 is greatly increased, do not exhibit a significant modification of their K_i for the natural hormone AVP and display only a small reduction in their affinities for SR49059 and [^{125}I]-HO-LVA (see Table 2). Results concerning the selective V_{1b} agonist d[Cha^4]AVP are slightly different. According to

Table 3. Functional Properties of Wild-Type and Mutant AVP Receptors for AVP and SSR149415

AVP Receptor	AVP (K_{act} nM)	SSR149415 (K_{inact} nM)
Wild-type receptors		
V_{1a}	0.96 ± 0.18	90.3 ± 5.7
V_{1b}	1.06 ± 0.05	0.95 ± 0.07
Mutant receptors		
M220T	0.75 ± 0.26	2.55 ± 0.11
A334M	3.41 ± 0.58	19.5 ± 4.5

Phospholipase C assays were performed as described in *Materials and Methods.* K_{act} and K_{inact} values for AVP and SSR149415, respectively, were obtained from the dose-response curves illustrated in Fig. 5. Results are the mean ± SEM of at least three separate experiments each performed in triplicate.

the mutant considered, we observed either a significant slight decrease (M220T) or increase (A334M) of their affinities for d[Cha^4]AVP. Such results would indicate that a mutation introduced in position 220 or 334 of the hV_{1a}-R directly or indirectly affects the interaction of this selective agonist with the mutant, in contrast to the nonselective agonist AVP (compare Tables 1 and 2). Such properties are probably in relation to the ability of AVP and d[Cha^4]AVP to differentially activate phospholipase C in CHO cells expressing the hV_{1a}-R (d[Cha^4]AVP being a partial agonist of this receptor subtype as compared with AVP; data not shown) and may reflect distinct interactions with the TM domains involved in the coupling to heterotrimeric G proteins. An accurate analysis of the residues involved in the binding of AVP and/or d[Cha^4]AVP to a putative active state model of AVP receptors is necessary to validate these assumptions and to verify whether the specificity of the V_{1b}-R subtype could not be assumed by specific residues located within the lower part of the TM domains, generally known to affect the coupling properties. All together, these experiments suggest that a single mutation of the hV_{1a}-R may strongly affect its binding properties shifting from a V_{1a} to a V_{1b} pharmacological profile. This may also explain why the V_{1a} and V_{1b} receptor isoforms are phylogenetically so closed. In contrast to the V_2-R isoform, they share the ability to activate phospholipases C via a $G_{q/11}$ heterotrimeric G protein and differ especially by the structure of their binding site for antagonists such as SSR149415.

If the upper part of the TM helices of the group 1 GPCR family (including the AVP/OT receptors) are known to form a binding pocket for their specific ligands (32), a contribution of their extracellular loops to ligand selectivity has also been demonstrated. Hence the residue 115, located at the border between TM2 and the first extracellular domain, plays a key role in the pharmacological properties of the V_{1a}, V_2, and oxytocin receptor subtypes (13). Similarly, the E2 loop of the hV_2-R isoform represents an important structural motif for discriminating between V_2 agonist and antagonist (15).

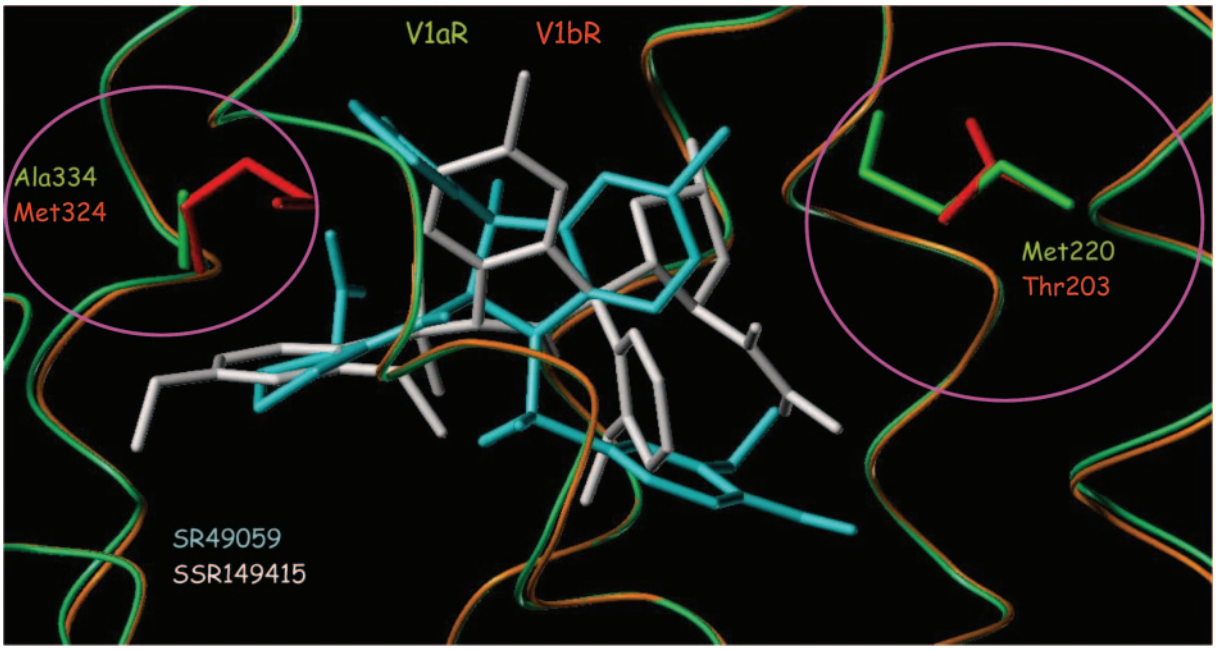

Fig. 6. Hypothesized Binding Mode of the Selective V_{1a} Antagonist SR49059 (*cyan sticks*) to the V_{1a}-R Model (*green ribbons*) and of the Selective V_{1b} Antagonist SSR149415 (*white sticks*) to the V_{1b}-R Model (*orange ribbons*)

The two main differing amino acids of the TM binding cavity are *circled* and displayed as *solid sticks*.

As the E2 loop from the three AVP receptor isoforms is quite different in terms of amino acid sequence, as compared with the first and third extracellular loops, we decided to verify whether this extracellular domain may control the ligand accessibility to the binding pocket (see Ref. 29) and could play a role in the hV_{1b}-R selectivity. A chimeric hV_{1a}-R, the E2 loop of which was replaced by that of the hV_{1b}-R ($V_{1a}/E2V_{1b}$), was thus generated and tested for its binding selectivity. Despite a weak amino acid sequence homology between the hV_{1a}-R and hV_{1b}-R E2 loops (47%), no significant modification of the pharmacological properties of this chimera was observed as compared with the wild-type hV_{1a}-R. Yet, on the basis of these experiments performed at equilibrium, we cannot totally exclude a potential role of the E2 loop.

This structural information concerning the hV_{1b}-R with respect to those previously described for the V_{1a} and V_2 receptors, allow interesting comparisons regarding the binding site of specific AVP receptor antagonists. For the three AVP receptor subtypes, various peptide and nonpeptide antagonists were shown to interact with amino acids mainly located at the top of TM domains (15–17, 19), suggesting that the binding sites of these ligands are localized in a binding cleft formed by the upper part of these α-helical domains. Interestingly, the amino acids responsible for the AVP receptors selectivity toward antagonists varied from one isoform to another. Thus, to date, we know that these residues are located on TM domains 5 and 7 for the V_{1b}-R (present study) on TM domains 2, 3, 4, 6, and 7 for the V_{1a}-R (16, 19) and restricted to the seventh helix for the V_2-R (15).

Obviously, as indicated before, the knowledge of the residues of the V_{1b}-R allowing the binding discrimination between agonists and antagonists is also important. The results reported here clearly show that the Thr203 and Met324 residues are involved mainly in the binding of specific V_{1b} antagonist because the M220T and A334M V_{1a} mutants both exhibited strong increases in affinity for SSR149415 without important K_d/K_i modifications for AVP and d[Cha^4]AVP. Yet, further investigations will be necessary to accurately localize the molecular determinants that define agonist binding into the hV_{1b}-R.

In conclusion, these first results about the hV_{1b}-R functional architecture, allow a better virtual screening of new selective V_{1b} antagonists. Such new compounds are of potential therapeutic interest because, as previously observed, SSR149415, the first designed V_{1b} antagonist, reduced the level of stress and anxiety in the rat as efficiently as classical benzodiazepines with perhaps a safer profile (20).

MATERIALS AND METHODS

Chemicals

Most standard chemicals were purchased from Sigma Chemical Co. (St. Louis, MO), Roche Molecular Biochemicals (Mannheim, Germany), or Merck & Co., Inc. (Darmstadt, Germany), unless otherwise indicated. AVP came from Bachem (Bubendorf, Switzerland). SSR149415, SR49059, and SR121463 were from Sanofi-Synthelabo Laboratories (Montpellier, France). [^{3}H]AVP (60–80 Ci/mmol), was from Perkin-Elmer Life Sciences (Courtaboeuf, France). HO-LVA was a

generous gift of Professor Maurice Manning. Unlabeled HO-LVA was radioiodinated to give [^{125}I]-HO-LVA ([HO]phenylacetyl-D-Tyr(Me)^2-Phe^3-Gln^4,Asn^5,Arg^6-Pro^7-Arg^8-NH_2) as previously described (33). DMEM, penicillin-streptomycin, L-glutamine, and nonessential amino acids were purchased from Invitrogen (Cergy Pontoise, France). Inositol-free DMEM came from ICN Biochemicals (Orsay, France). Dowex AG1-X8 (formate form, 200–400 mesh) was purchased from Bio-Rad Laboratories, Inc. (Munchen, Germany).

Alignment of Amino Acid Sequences

The amino acid sequences of the human V_{1a} and V_{1b} AVP receptor subtypes were retrieved from the Swiss-Prot database (accession nos.: V_{1a}-R, P37288; V_{1b}-R, P47901) and aligned to the sequence of bovine rhodopsin (accession no. P02699) using the in-house developed GPCRmod program (34) focusing on TM domains only. The alignment of the amino- and carboxy-terminal domains as well as of the intra- and extracellular loops was realized using ClustalW (35). A slow pair-wise alignment using BLOSUM matrix series (36) and a gap opening penalty of 15.0 were chosen for aligning the amino acid sequences to the sequence of bovine rhodopsin.

Modeling the Antagonist-Bound State of the hV_{1b}-R

The 3D model of the hV_{1b}-R was constructed from a previously reported model of the hV_{1a}-R (25) by mutating the side chains of the amino acids of the V_{1a}-R. Standard geometries for the mutated side chains were given by the BIOPOLYMER module of SYBYL (37). Whenever possible, the side chain torsional angles were kept to the values occurring in the V_{1a}-R model. Otherwise, a short scanning of side chain angles was performed to remove steric clashes between the mutated side chain and the other amino acids. The third intracellular loop between helices 5 and 6, which shows a high degree of variability, was not included in the model. This loop is probably not involved in direct interactions with the ligand as it was previously observed on the V_{1a}-R model (25). We therefore assumed that omitting this loop should not influence our docking results. Insertions/deletions occurred only in loops but not in secondary structure elements (α-helix, β-sheet). The insertions/deletions in the loops were achieved through a simple knowledge-based loop search procedure using the LOOPSEARCH module of the SYBYL package (37). In this procedure, a set of 1478 high-resolution x-ray structures was searched for loops of similar length and similar distance between the Cα atoms of the residues delimiting the loop window. The loop showing the highest sequence identity and the lowest root-mean square (rms) deviations was then selected for insertion in the model. After the heavy atoms were modeled, all hydrogen atoms were added, and the protein coordinates were then minimized with AMBER (38) using the AMBER95 force field (39). Topology and charge parameters for the nonpeptide V_{1b} antagonist were computed using a previously described procedure (40). The minimizations were carried out by 1000 steps of steepest descent followed by conjugate gradient minimization until the rms gradient of the potential energy was less than 0.05 kcal/mol.Å. A twin cut-off (10.0, 15.0 Å) was used to calculate nonbonded electrostatic interactions at every minimization step, and the nonbonded pair list was updated every 25 steps. A distance-dependent ($\epsilon = 4r$) dielectric function was used.

Automated Docking of a Selective V_{1b} Antagonist (SSR149415)

The Gold 1.2 docking program (41) was used to automatically dock the selective V_{1b} antagonist SSR149415. For each of the 10 independent genetic algorithm (GA) runs, a maximum number of 1000 GA operations was performed on a single population of 50 individuals. Operator weights for cross-over, mutation, and migration were set to 100, 100, and 0, respectively. To allow poor nonbonded contacts at the start of each GA run, the maximum distance between hydrogen donors and fitting points was set to 5 Å, and nonbonded van der Waals energies were cut off at a value equal to k_{ij} (well depth of the van der Waals energy for the atom pair i,j). To further speed up the calculation, the GA docking was stopped when the top three solutions were within 1.5 Å rms deviations. If this criterion is met, we can assume that these top solutions represent a reproducible pose for the ligand.

Site-Directed Mutagenesis

All the mutations were generated into the hV_{1a}-R sequence. The pRK5 expression vector containing the hV_{1a}-R cDNA and the ampicillin resistance gene was kindly provided by Dr. B Mouillac. Amino acid replacements were generated by PCR using the QuikChange site-directed mutagenesis kit, according to the manufacturer's protocol (Stratagene, La Jolla, CA). For single-amino acid replacements (L181F, M220T, A334M, and S338N), cDNA of the wild-type hV_{1a}-R was used as the template with the appropriate mutated oligonucleotides primers. The double mutant M220T/A334M was generated as described above using cDNA of the M220T mutant as the template and mutated oligonucleotides primers corresponding to the A334M mutation. PCR products were transformed into the *Escherichia coli* XL-1 blue bacteria strain, and positive clones were selected under ampicillin selection. Plasmidic cDNAs of positive clones were then purified with the QIAprep Spin Miniprep Kit (QIAGEN, Courtaboeuf, France). All the mutations were verified by sequencing (Genome Express, Meylan, France). For further amplification of positive clones the *E. coli* DH_5-α bacteria strain (Invitrogen) was used.

Construction of the Chimeric V_{1a}-R Containing the V_{1b} E2 Loop

Modifications were performed in the hV_{1a}-R cDNA inserted into the pRK5 expression vector containing the ampicillin resistance gene. *Afl*II and *Xho*I enzymatic cleavage sites were respectively introduced at the 3′- and 5′-ends of the E2 loop of the hV_{1a}-R cDNA by site-directed mutagenesis with the appropriate oligonucleotides primers. These mutations were silent because they did not modify the amino acid sequence of the wild-type V_{1a}-R. Specific digestion of each side of the V_{1a} E2 loop with appropriate restriction enzymes was done, and an oligonucleotide sequence corresponding to the E2 loop of the hV_{1b}-R was then introduced by T4 ligase treatment. Each construct was transformed, grown, and ampicillin selected into the *E. coli* DH_5-α bacteria strain. All the constructs were verified by sequencing (Genome Express).

cDNA Expression of Wild-Type and Mutant AVP Receptors and Cell Culture

The human V_{1a} and V_{1b} wild-type receptors were stably expressed in Chinese Hamster Ovary cells (CHO) as previously described (16). The mutants and chimera of the hV_{1a}-R were transiently expressed in CHO cells by electroporation. Briefly, the cells (10^7/0.3 ml) were suspended in an electroporation buffer containing: 50 mM K_2HPO_4; 20 mM $C_2H_3KO_2$; 20 mM KOH, pH 7.4; 20 μg of carrier DNA (pRK5 expression vector without any insert); 0.5–2μg of the expression vector containing the mutated receptor cDNA and 40 mM $MgSO_4$; and then incubated for 20 min at room temperature before being pulsed (280 V, 950 μF, Bio-Rad Apparatus).

The CHO cells expressing the wild-type and mutated AVP receptors were plated in 150-mm Petri dishes or 24-well

plates depending upon the experiment to be conducted. Cells were maintained in culture in DMEM supplemented with 10% fetal calf serum, 2 mM L-glutamine, 500 U/ml penicillin and streptomycin, and nonessential amino acids in an atmosphere of 95% air and 5% CO2 at 37 C. Cells were used 48 h after seeding both for binding and functional assays.

Membrane Preparations

CHO cells stably or transiently transfected with the wild-type or the mutated AVP receptors were harvested, washed two times in PBS without calcium and magnesium, Polytron homogenized in lysis buffer (15 mM Tris-HCl, pH 7.4; 2 mM $MgCl_2$, 0.3 mM EDTA), and centrifuged at 100 $\times$ *g* for 5 min at 4 C. The supernatants were recovered and centrifuged at 44,000 $\times$ *g* for 20 min at 4 C. The pellets were washed in 50 mM Tris-HCl (pH 7.4)-3 mM $MgCl_2$ (buffer A) and centrifuged at 44,000 $\times$ *g* for 20 min at 4 C. The membranes were suspended in a small volume of buffer A and their protein contents were determined. Aliquots of membranes were used immediately or stored at −80 C.

Radioligand-Binding Assay

Membrane-binding assays were performed at 30 C as described previously (42) with [^{3}H]AVP or [^{125}I]HO-LVA as radioligands. Affinities of [^{3}H]AVP and [^{125}I]-HO-LVA (K_d) for the wild-type and the mutated AVP receptors were determined in saturation experiments using concentrations ranging from 0.1 to 10 nM and 10 to 1500 pM, respectively. For each concentration of radioligand, total and nonspecific binding were determined in the absence or presence of 1 μM of unlabeled AVP, respectively. Affinities of the unlabeled ligands (K_i) were determined in competition experiments using 0.5 to 1 nM [^{3}H]AVP (a concentration close to the K_d value of the wild-type or the mutated receptors studied) and increasing concentrations of the unlabeled analogs to be tested (0.1 nM to 10 μM). Radioactivity found associated to plasma membranes was determined by filtration through GF/C filters, and specific binding was calculated as previously described (42).

IP Assays

Total IP accumulation was determined as previously described (43). Briefly, CHO cells stably or transiently transfected with the wild-type and the mutated receptors were grown for 24 h in DMEM supplemented with 10% fetal calf serum. Cells were further incubated for another 24-h period in a serum and inositol-free medium supplemented with 1 μCi·ml^{-1} myo-[2-^{3}H]inositol. Cells were then washed twice with a Hanks' buffered saline (HBS) medium. For stimulation experiments, the cells were preincubated for 15 min in HBS supplemented with 20 mM LiCl and further stimulated for 15 min with the agonists to be tested. For inhibition experiments, the cells were preincubated 15 min with HBS/LiCl medium supplemented with the antagonist to be tested and further stimulated for 15 min with 1 nM AVP. The reaction was stopped by adding perchloric acid (5% vol/vol). Total IPs accumulated were extracted, purified on Dowex AG1-X8 anion exchange chromatography column, and counted.

Data Analysis

The radioligand binding data were analyzed by GraphPad Prism (GraphPad Software, Inc., San Diego, CA). The K_d values of the radioligands were determined according to the Scatchard linearization of the saturation curve obtained (44). The K_i values for unlabeled analogs were calculated from binding competition experiments according to the Cheng and Prusoff equation (45): $K_i = IC_{50} \times (K_d/K_d+[L])$, where IC_{50} is the concentration of unlabeled analog leading to half-maximal inhibition of specific binding, [L] is the concentration of the radioligand present in the assay, and K_d is its affinity for the receptor studied. Concentrations of analog leading to half-maximal stimulation (K_{act}) or inhibition (K_{inact}) of IP accumulation were calculated from functional studies using GraphPad PRISM. Results are expressed as the mean $\pm$ SEM of the number of distinct experiments indicated.

Acknowledgments

We are grateful to Professor Maurice Manning for providing many structural analogs of AVP and Dr. Claude Barberis for radioiodination of HO-LVA. Many thanks to Mireille Passama for her excellent work in preparing the illustrations.

Received March 24, 2004. Accepted July 21, 2004.

Address all correspondence and requests for reprints to: Guillon Gilles, Institut National de la Santé et de la Recherche Médicale Unité 469, 141 rue de la Cardonille, 34094 Montpellier, Cedex 05, France. E-mail: gilles.guillon@ccipe.cnrs.fr.

This work was supported by Institut National de la Santé et de la Recherche Médicale (to G.G.), Fondation pour la recherche médicale (to S.D.), Centre National de la Recherche Scientifique, and Genopole Alsace-Lorraine (to M.H. and D.R.).

REFERENCES

1. Jard S 1998 Vasopressin receptors. A historical survey. Adv Exp Med Biol 449:1–13
2. Guillon G, Grazzini E, Andrez M, Breton C, Trueba M, Serradeil-Le Gal C, Boccara G, Derick S, Chouinard L, Gallo-Payet N 1998 Vasopressin: a potent autocrine/paracrine regulator of mammal adrenal functions. Endocr Res 24:703–710
3. Gao ZY, Gerard M, Henquin JC 1992 Glucose- and concentration-dependence of vasopressin-induced hormone release by mouse pancreatic islets. Regul Pept 38:89–98
4. Manning PT, Schwartz D, Katsube NC, Holmberg SW, Needleman P 1985 Vasopressin-stimulated release of atriopeptin: endocrine antagonists in fluid homeostasis. Science 229:395–397
5. Barberis C, Tribollet E 1996 Vasopressin and oxytocin receptors in the central nervous system. Crit Rev Neurobiol 10:119–154
6. Serradeil-Le Gal C, Wagnon J, Simiand J, Griebel G, Lacour C, Guillon G, Barberis C, Brossard G, Soubrie P, Nisato D, Pascal M, Pruss R, Scatton B, Maffrand JP, Le Fur G 2002 Characterization of (2S,4R)-1-[5-chloro-1-[(2,4-dimethoxyphenyl)sulfonyl]-3-(2-methoxy-phenyl)-2-oxo-2,3-dihydro-1H-indol-3-yl]-4-hydroxy-N,N-dimethyl-2-pyrrolidine carboxamide (SSR149415), a selective and orally active vasopressin V1b receptor antagonist. J Pharmacol Exp Ther 300:1122–1130
7. Thibonnier M, Coles P, Thibonnier A, Shoham M 2002 Molecular pharmacology and modeling of vasopressin receptors. Prog Brain Res 139:179–196
8. Thibonnier M, Berti-Mattera LN, Dulin N, Conarty DM, Mattera R 1998 Signal transduction pathways of the human V1-vascular, V2-renal, V3-pituitary vasopressin and oxytocin receptors. Prog Brain Res 119:147–161

9. Barberis C MD, Durroux T, Mouillac B, Guillon G, Seyer R, Hibert M, Tribollet E, Manning M 1999 Molecular pharmacology of AVP and OT receptors and therapeutic potential. Drug News Perspect 12:279–298
10. Thibonnier M, Coles P, Thibonnier A, Shoham M 2001 The basic and clinical pharmacology of nonpeptide vasopressin receptor antagonists. Annu Rev Pharmacol Toxicol 41:175–202
11. Derick S, Cheng LL, Voirol MJ, Stoev S, Giacomini M, Wo NC, Szeto HH, Ben Mimoun M, Andres M, Gaillard RC, Guillon G, Manning M 2002 [1-Deamino-4-cyclohexylalanine] arginine vasopressin: a potent and specific agonist for vasopressin V1b receptors. Endocrinology 143: 4655–4664
12. Mouillac B, Chini B, Balestre MN, Elands J, Trumpp-Kallmeyer S, Hoflack J, Hibert M, Jard S, Barberis C 1995 The binding site of neuropeptide vasopressin V1a receptor. Evidence for a major localization within transmembrane regions. J Biol Chem 270:25771–25777
13. Chini B, Mouillac B, Ala Y, Balestre MN, Trumpp-Kallmeyer S, Hoflack J, Elands J, Hibert M, Manning M, Jard S, Barberis C 1995 Tyr115 is the key residue for determining agonist selectivity in the V1a vasopressin receptor. EMBO J 14:2176–2182
14. Hawtin SR, Wesley VJ, Parslow RA, Simms J, Miles A, McEwan K, Wheatley M 2002 A single residue (arg46) located within the N-terminus of the V1a vasopressin receptor is critical for binding vasopressin but not peptide or nonpeptide antagonists. Mol Endocrinol 16: 600–609
15. Cotte N, Balestre MN, Phalipou S, Hibert M, Manning M, Barberis C, Mouillac B 1998 Identification of residues responsible for the selective binding of peptide antagonists and agonists in the V2 vasopressin receptor. J Biol Chem 273:29462–29468
16. Phalipou S, Cotte N, Carnazzi E, Seyer R, Mahe E, Jard S, Barberis C, Mouillac B 1997 Mapping peptide-binding domains of the human V1a vasopressin receptor with a photoactivatable linear peptide antagonist. J Biol Chem 272:26536–26544
17. Phalipou S, Seyer R, Cotte N, Breton C, Barberis C, Hibert M, Mouillac B 1999 Docking of linear peptide antagonists into the human V(1a) vasopressin receptor. Identification of binding domains by photoaffinity labeling. J Biol Chem 274:23316–23327
18. Thibonnier M, Coles P, Conarty DM, Plesnicher CL, Shoham M 2000 A molecular model of agonist and nonpeptide antagonist binding to the human V(1) vascular vasopressin receptor. J Pharmacol Exp Ther 294: 195–203
19. Cotte N, Balestre MN, Aumelas A, Mahe E, Phalipou S, Marin D, Hibert M, Manning M, Durroux T, Barberis C, Mouillac B 2000 Conserved aromatic residues in the transmembrane region VI of the V1a vasopressin receptor differentiate agonist vs. antagonist ligand binding. Eur J Biochem 267:4253–4263
20. Griebel G, Simiand J, Serradeil-Le Gal C, Wagnon J, Pascal M, Scatton B, Maffrand JP, Soubrie P 2002 Anxiolytic- and antidepressant-like effects of the non-peptide vasopressin V1b receptor antagonist, SSR149415, suggest an innovative approach for the treatment of stress-related disorders. Proc Natl Acad Sci USA 99: 6370–6375
21. Wersinger SR, Ginns EI, O'Carroll AM, Lolait SJ, Young III WS 2002 Vasopressin V1b receptor knockout reduces aggressive behavior in male mice. Mol Psychiatry 7:975–984
22. Grazzini E, Lodboerer AM, Perez-Martin A, Joubert D, Guillon G 1996 Molecular and functional characterization of V1b vasopressin receptor in rat adrenal medulla. Endocrinology 137:3906–3914
23. Lee B, Yang C, Chen TH, al-Azawi N, Hsu WH 1995 Effect of AVP and oxytocin on insulin release: involvement of V1b receptors. Am J Physiol 269: E1095–E1100
24. Attwood TK 2001 A compendium of specific motifs for diagnosing GPCR subtypes. Trends Pharmacol Sci 22: 162–165
25. Bissantz C, Bernard P, Hibert M, Rognan D 2003 Protein-based virtual screening of chemical databases. II. Are homology models of G-protein coupled receptors suitable targets? Proteins 50:5–25
26. Tahtaoui C, Balestre MN, Klotz P, Rognan D, Barberis C, Mouillac B, Hibert M 2003 Identification of the binding sites of the SR49059 nonpeptide antagonist into the V1a vasopressin receptor using sulfydryl-reactive ligands and cysteine mutants as chemical sensors. J Biol Chem 278: 40010–40019
27. Serradeil-Le Gal C, Wagnon J, Garcia C, Lacour C, Guiraudou P, Christophe B, Villanova G, Nisato D, Maffrand JP, Le Fur G, Guillon G, Cantau B, Barberis C, Trueba M, Ala Y, Jard S 1993 Biochemical and pharmacological properties of SR 49059, a new, potent, nonpeptide antagonist of rat and human vasopressin V1a receptors. J Clin Invest 92:224–231
28. Serradeil-Le Gal C, Lacour C, Valette G, Garcia G, Foulon L, Galindo G, Bankir L, Pouzet B, Guillon G, Barberis C, Chicot D, Jard S, Vilain P, Garcia C, Marty E, Raufaste D, Brossard G, Nisato D, Maffrand JP, Le Fur G 1996 Characterization of SR 121463A, a highly potent and selective, orally active vasopressin V2 receptor antagonist. J Clin Invest 98:2729–2738
29. Palczewski K, Kumasaka T, Hori T, Behnke CA, Motoshima H, Fox BA, Le Trong I, Teller DC, Okada T, Stenkamp RE, Yamamoto M, Miyano M 2000 Crystal structure of rhodopsin: a G protein-coupled receptor. Science 289:739–745
30. Ballesteros JA, Shi L, Javitch JA 2001 Structural mimicry in G protein-coupled receptors: implications of the high-resolution structure of rhodopsin for structure-function analysis of rhodopsin-like receptors. Mol Pharmacol 60: 1–19
31. Petrel C, Kessler A, Maslah F, Dauban P, Dodd RH, Rognan D, Ruat M 2003 Modeling and mutagenesis of the binding site of Calhex 231, a novel negative allosteric modulator of the extracellular Ca^{2+}-sensing receptor. J Biol Chem 278:49487–49494
32. Bockaert J, Pin JP 1999 Molecular tinkering of G protein-coupled receptors: an evolutionary success. EMBO J 18:1723–1729
33. Barbeis C, Balestre MN, Jard S, Tribollet E, Arsenijevic Y, Dreifuss JJ, Bankowski K, Manning M, Chan WY, Schlosser SS, Holsboer F, Elands J 1995 Characterization of a novel, linear radioiodinated vasopressin antagonist: an excellent radioligand for vasopressin V1a receptors. Neuroendocrinology 62:135–146
34. Bissantz C, Logean A, Rognan D 2004 High-throughput modeling of human G protein coupled receptors: amino acid sequence alignment, three dimensional model building, and receptor library screening. J Chem Inf Comput Sys 44:1162–1176
35. Thompson JD, Higgins DG, Gibson TJ 1994 CLUSTAL W: improving the sensitivity of progressive multiple sequence alignment through sequence weighting, position-specific gap penalties and weight matrix choice. Nucleic Acids Res 22:4673–4680
36. Henikoff S, Henikoff JG 1992 Amino acid substitution matrices from protein blocks. Proc Natl Acad Sci USA 89:10915–10919
37. SYBYL 6.9 release, St. Louis, MO: TriPOS Assoc., Inc. (software manual)

38. Case DA, Pearlman DA, Caldwell JW, CheathamTE, Ross WS, Simmerling CL, Darden TA, Merz JKM, Stanton RV, Cheng AL, Vincent JJ, Crowley M, Ferguson DM, Radmer RJ, Seibel GL, Singh UC, Weiner PK, Kollman PA 1997 AMBER 6.0 release, San Francisco University (software manual)
39. Cornell WD, Cieplak P, Bayly CI, Gould IR, Merz KM, Ferguson DM, Spellmeyer DC, Fox T, Caldwell JW, Kollman PA 1995 A second generation force field for the simulation of proteins, nucleic acids, and organic molecules. J Am Chem Soc 117:5179–5197
40. Rognan D, Mukhija S, Folkers G, Zerbe O 2001 NMR-restrained docking of a peptidic inhibitor to the N-terminal domain of the phosphoenolpyruvate:sugar phosphotransferase enzyme I. J Comput Aided Mol Des 15:103–115
41. Jones G, Willett P, Glen RC, Leach AR, Taylor R 1997 Development and validation of a genetic algorithm for flexible docking. J Mol Biol 267:727–748
42. Andres M, Trueba M, Guillon G 2002 Pharmacological characterization of F-180: a selective human V(1a) vasopressin receptor agonist of high affinity. Br J Pharmacol 135:1828–1836
43. Guillon G, Trueba M, Joubert D, Grazzini E, Chouinard L, Cote M, Payet MD, Manzoni O, Barberis C, Robert M, Gallo-Payet N 1995 Vasopressin stimulates steroid secretion in human adrenal glands: comparison with angiotensin-II effect. Endocrinology 136:1285–1295
44. Weder HG, Schildknecht J, Lutz RA, Kesselring P 1974 Determination of binding parameters from Scatchard plots. Theoretical and practical considerations. Eur J Biochem 42:475–481
45. Cheng Y, Prusoff WH 1973 Relationship between the inhibition constant (K1) and the concentration of inhibitor which causes 50 per cent inhibition (I_{50}) of an enzymatic reaction. Biochem Pharmacol 22:3099–3108

Molecular Endocrinology **is published monthly by The Endocrine Society (http://www.endo-society.org), the foremost professional society serving the endocrine community.**